**Article:**
Wilson, TW, Ladino, LA, Alpert, PA et al. (26 more authors) (2015) A marine biogenic source of atmospheric ice nucleating particles. Nature, 525 (7568). pp. 234-238. ISSN 0028-0836

https://doi.org/10.1038/nature14986

# A marine biogenic source of atmospheric ice nucleating particles

T.W. Wilson[1*], L.A. Ladino[2*], P.A. Alpert[3], M.N. Breckels[4], I.M. Brooks[1], J. Browse[1], S.M. Burrows[5], K.S. Carslaw[1], J.A. Huffman[6], C. Judd[1], W.P. Kilthau[7], R.H. Mason[8], G. McFiggans[9], L.A Miller[10], J.J. Nájera[9], E. Polishchuk[8], S. Rae[9], C.L. Schiller[11], M. Si[8], J. Vergara Temprado[1], T.F. Whale[1], J.P.S. Wong[2], O. Wurl[12], J.D. Yakobi-Hancock[2], J.P.D. Abbatt[2], J.Y. Aller[7], A.K. Bertram[8], D.A. Knopf[3], and B.J. Murray[1]

[1]School of Earth and Environment, University of Leeds, Woodhouse Lane, Leeds, LS2 9JT, UK

[2]Department of Chemistry, University of Toronto, 80 St. George St., Toronto, Ontario, M5S 3H6, Canada

[3]Institute for Terrestrial and Planetary Atmospheres, School of Marine and Atmospheric Sciences, Stony Brook University, Stony Brook, NY 11794-5000, USA

[4]School of Biological Sciences, University of Essex, Colchester, CO4 3SQ UK

[5]Atmospheric Science and Global Change Division, Pacific Northwest National Laboratory,, 902 Battelle Boulevard, Richland, WA 99354, United States

[6]Department of Chemistry and Biochemistry, University of Denver, Denver, 80208, Colorado, USA

[7]School of Marine and Atmospheric Sciences, Stony Brook University, Stony Brook, NY 11794-5000, USA

[8]Department of Chemistry, University of British Columbia, 2036 Main Mall, Vancouver, BC, V6T 1Z1, Canada

[9]School of Earth, Atmospheric and Environmental Sciences, University of Manchester, Manchester, M13 9PL, UK

[10]Institute of Ocean Sciences, Fisheries and Oceans Canada, Sidney, BC V8L 4B2 Canada

[11]Air Quality Science Unit, Environment Canada, Vancouver, BC, V6C 3S5, Canada

[12]Leibniz Institute for Baltic Sea Research Warnemünde, Department of Biological Oceanography, Germany

[*]T.W.W. and L.A.L. contributed equally to this work

**The amount of ice present in clouds can affect cloud lifetime, precipitation and radiative properties[1,2]. The formation of ice in clouds is facilitated by the presence of airborne ice nucleating particles[1,2]. Sea spray is one of the major global sources of atmospheric particles, but it is unclear to what extent these particles are capable of nucleating ice[3-11]. Sea spray aerosol contains large amounts of organic material that is ejected into the atmosphere during bubble bursting at the organically enriched sea-air interface or sea surface microlayer[12-19]. Here we show that organic material in the sea surface microlayer nucleates ice under conditions relevant for mixed-phase cloud and high-altitude ice cloud formation. The ice nucleating material is likely biogenic and less than ~0.2 µm in size. We find that exudates separated from cells of the marine diatom T. Pseudonana nucleate ice and propose that organic material associated with phytoplankton cell exudates is a likely candidate for the observed ice nucleating ability of the microlayer samples. Global model simulations of marine organic aerosol in combination with our measurements suggest that marine organic material may be an important source of ice nucleating particles in remote marine environments such as the Southern Ocean, North Pacific and North Atlantic.**

Atmospheric ice nucleating particles (INPs) allow ice to nucleate heterogeneously at higher temperatures or lower relative humidity than is typical for homogeneous ice nucleation. Heterogeneous ice nucleation proceeds via different pathways depending on temperature and humidity. In low altitude mixed-phase clouds, INPs are commonly immersed in supercooled liquid droplets and freezing can occur on them at temperatures between -36 and 0°C[2]. At higher altitudes and lower temperatures (<-36°C) where cirrus clouds form, nucleation occurs below water saturation, proceeding by homogeneous, deposition or immersion-in-solution nucleation[1]. Understanding the sources of atmospheric INPs is important because they affect cloud lifetime, cloud albedo and precipitation[1,2]. Recent modelling work has shown that the ocean is potentially an important source of biogenic atmospheric INPs particularly in remote, high latitude regions[9,10]. However, it has never been directly shown that there is a source of atmospheric INPs associated with organic material found in marine waters or sea-spray aerosol.

Organic material makes up a substantial fraction of sub-micron sea-spray aerosol and it is estimated that 10±5 Tg $yr^{-1}$ of primary organic sub-micron aerosol is emitted from marine sources globally[12]. Rising bubbles scavenge surface active organic material from the water column at their interfaces and this process facilitates the formation of the organic enriched sea-air interface known as the sea surface microlayer (SML). This organic material is ejected into the atmosphere during bubble bursting resulting in sea spray aerosol containing similar organic material to that of the microlayer[12–19] (Figure 1). Measurements of atmospheric INP concentrations in the remote oceans indicate that there may be a marine source of INPs linked to marine biology[3–5], and modelling work indicates that this may be important in mixed phase clouds[9,10]. There is also evidence to suggest that ice nucleation in cirrus clouds over ocean regions is influenced by sea spray aerosol, with about 25% of the heterogeneously nucleated ice particle residuals identified as sea salt[20]. Despite these indications that there is a marine source of atmospheric INPs, the sea surface microlayer has not previously been analysed for the presence of material capable of nucleating ice. To determine if there is a source of atmospheric INPs in the microlayer, we have examined the ice nucleating properties of microlayer samples collected in the Arctic (July-August 2013), Atlantic (May-June, 2014), North Pacific (June, 2013), and in coastal locations off British Columbia, Canada (August 2013) (Extended data Figure 1).

First we present experiments relevant to mixed-phase clouds, in which 1 µl droplets of microlayer samples from the Arctic and Atlantic Oceans were placed on a cold stage immediately after sampling, and cooled until frozen. The fraction of droplets that froze as a function of temperature, corrected for freezing depression caused by salts, is shown in Figure 2a. The microlayer droplets consistently froze at higher temperatures than droplets of sub-surface water (SSW) collected at depths of between 2 - 5 m at the same locations (Extended data Table 1). Filtration and re-testing of the microlayer samples showed that most material which nucleated ice was between approximately 0.2 and 0.02 µm in size (Extended data Figure 2a). Material of this size has the potential to be lofted into the atmosphere through bubble bursting processes, forming atmospheric INPs which are internally mixed with sea salt and other organics. In order to estimate atmospheric INP concentrations associated with marine organics we determined the number of these INPs present per mass of organic carbon (Figure 2b; see methods); this result is used in the modelling section of this paper.

Experiments were also conducted under conditions relevant to cirrus clouds using microlayer and sub-surface water samples from the North Pacific and the British Columbia (BC) coast. The activity of the collected samples was tested at -40°C and compared with results from experiments with commercial sea salt and NaCl particles. Figure 2c shows example activation curves for aerosolised, dried and size selected (200 nm diameter) particles. The sub-surface water activation curves are very similar to those of sea salt and NaCl, with all showing sharp increases above 143% relative humidity with respect to ice ($RH_{ice}$). This is consistent with homogeneous ice nucleation of solution droplets and suggests that crystalline salt particles did not contribute significantly to ice nucleation events observed at low $RH_{ice}$. In contrast, aerosol particles derived from microlayer samples all showed ice formation above the background level at lower $RH_{ice}$. The ice nucleation onset ($RH_{ice}$ at which 1% of the aerosol particles were activated, Figure 2d) varied between 115 and 133% $RH_{ice}$ which is comparable with efficient deposition mode INPs such as Arizona test dust (ATD) and feldspar dust (orthoclase) particles of the same size[1,21]. Filtration of the SML samples through filters with nominal pore sizes of 0.2 µm, increased the ice nucleation onset by about 12-16±4% $RH_{ice}$, indicating that some ice active material larger than 0.2 µm was present (Extended data Figure 2b). However, the onsets for the 0.2 µm filtered samples remained well below the homogeneous threshold, indicating that there is a population of smaller INPs in the BC and Pacific microlayer samples, consistent with the Arctic and Atlantic data. The cumulative number of ice nucleation sites per surface area as a function of $RH_{ice}$, $n_s(RH_{ice})$, was greater for the microlayer samples than that found for ATD, kaolinite and feldspar mineral dusts[21,22] (Extended data Figure 3, see literature for more information on $n_s$[1,2]).

We emphasise that due to the different nucleation processes involved, ice nucleation under mixed-phase cloud and cirrus conditions cannot be quantitatively compared. Our results however do clearly show that the microlayers at all the sampling locations were enriched in INPs compared to the sub-surface water at the

same locations. In the following sections we present experiments designed to reveal likely candidates for the source of the ice nucleating activity.

Certain proteins have been identified as being highly ice active, however heat denatures proteins, causing a reduction in activity unlike known inorganic INPs[2]. To test if similar thermally labile material could be responsible for the observed ice nucleation, microlayer samples were heated at temperatures up to 100°C and retested for activity. Heating of Arctic and Atlantic samples resulted in a reduction of the ice nucleation activity with freezing shifting to lower temperatures (Extended data Figure 2c). Similarly, the onset $RH_{ice}$ of a BC coast sample increased by 6±4% $RH_{ice}$, whereas that of a Pacific sample was within uncertainty of the unheated sample (Extended data Figure 2b). This might be consistent with the presence of inorganic or other non-thermally labile INPs. The significant reduction in activity in samples from three out of four locations is consistent with the presence of thermally labile biological INPs.

The filtration tests on the sampled microlayers (mentioned above) show that there is a significant population of INPs which pass through 0.2 µm filters (Extended data Figure 2a and b). The ice active materials are therefore most likely smaller biological particles, e.g. ultramicrobacteria, viruses or extracellular material from phytoplankton or bacteria (exudate). Additionally, no correlation was found between freezing temperature and bacterial cell counts in the Arctic microlayer (Extended data Figure 4), which suggests that whole bacterial cells were not responsible for the observed ice nucleation. Given that terrestrial biological systems such as pollens[23,24] and fungi[25,26] have been found to produce nanoscale or 'macromolecular' INPs unconnected with whole cells, we considered the possibility that marine INPs are associated with exudates from phytoplankton or other marine microorganisms. This hypothesis is not only supported by the filtration tests, but by a tentative correlation between the North Pacific microlayer sample ice activation onsets with both the dissolved organic carbon concentration (DOC, >0.2 µm) and polysaccharide-rich transparent exopolymer particles (TEP) which are associated with phytoplankton exudates (Extended data Figure 5).

Qualitative compositional analysis of two Arctic samples using Scanning Transmission X-ray Microscopy coupled with Near Edge Absorption Fine Structure Spectroscopy (STXM/NEXAFS, Figure 3a-c) indicates the presence of both diatom cell wall and exudate compounds (see Methods). Spectra of exudates from the ubiquitous marine diatom *Thalassiosira pseudonana*[27] share absorption features with the microlayer samples. These data are in keeping with studies showing that diatom exudates are present in microlayer samples[18] and consistent with the fact that diatoms are the dominant phytoplanktonic group in polar regions[28].

Diatom cells and fragments have been shown to nucleate ice heterogeneously[6], but as demonstrated, whole cells are not solely responsible for the ice nucleation activity we observe in the microlayer samples. Here we investigate whether exudates separated from *T. pseudonana* diatom cells can nucleate ice heterogeneously. The ice nucleation efficiency of exudate from an axenic unialgal culture of *T. pseudonana* filtered through a 0.1 µm filter was measured as a function of temperature and water activity ($a_w$) in nanolitre volume droplets. Exudate freezing temperatures were found to be similar to those of washed diatom cells in the absence of exudate material and approximately 9 to 13°C warmer than observed homogeneous freezing temperatures of 0.2 µm filtered and autoclaved Atlantic seawater collected 100 km offshore of Long Island, NY (the same water used to culture diatoms) with and without added nutrients (Figure 3d, plus freezing curves shown in Extended data Figure 6). While the freezing temperatures shown in Figure 3d are not directly comparable to the microlayer droplet experiments in Figure 2a, as they used much smaller droplets, they do show that material associated with exudates can nucleate ice.

Given the ice nucleation activity of exudates from *T. pseudonana*, the presence of similar material in Arctic microlayer samples and the results of the filtering and heating experiments, we suggest that biogenic INPs present in phytoplankton exudates are a good candidate for the source of activity observed in the sampled microlayers. A significant mass fraction of sub-micron sea-spray aerosol is organic material[12,16] which is often associated with phytoplankton exudates[16,29]. Our results indicate therefore that some fraction of sea-spray aerosol particles will be capable of nucleating ice.

To explore the possible contribution of marine biogenic INP sources to the global atmospheric INP distribution we combined our experimental data with the modelled distribution of emitted primary organic material in sea spray aerosol[10] (Figure 4a, see methods for details). To calculate atmospheric INP concentrations we assume that the organic component of sea spray aerosol simulated by the model has a temperature-dependent INP concentration (per mass of organic carbon) equal to that measured in the Arctic and Atlantic samples (Figure 2b). In other words, the number of INP is directly related to the mass of OC computed by the model. At our current level of understanding, this can be considered as an estimate for the number of INPs present in the organic component of sea spray aerosol. The predicted surface level marine organic INP concentrations ($[INP]_{-15}$; the concentration of INP if an air parcel were cooled to -15$^{o}$C at water saturation) are shown in Figure 4a. The largest concentrations of marine INPs occur over the Southern Oceans, the North Atlantic and the North Pacific in regions where biological activity in surface ocean waters and wind speeds are greatest. Comparison of the simulated annual mean marine INP concentrations at sea level agree within ±1 order of magnitude with the Bigg[3] atmospheric INP measurements in the Southern Ocean and around the coast of Australia (Figure 4b), while mineral dust from deserts (the major terrestrial INP source) only accounts for a small fraction of the observed INPs in this region. We also find good agreement with measurements made by Rosinski and colleagues[4] in the southern Pacific. We note that some of the INP measurements by Rosinski in the equatorial Pacific tend to be under-predicted by our model, implying either another source of INPs or a stronger marine INP source than predicted here, possibly related to short-term variability in ocean biota.

We also use the model to assess the transport of marine INP to altitudes relevant for mixed-phase clouds. Figure 4c shows the concentration of INPs active at -20°C from marine sources at 850 hPa in comparison to the contribution from desert dusts based on K-feldspar distributions[30]. This suggests that marine biogenic sources of INPs are competitive with, or more important than, desert sources in large parts of the Southern Ocean, the North Atlantic and the North Pacific. In order to assess whether marine organic INPs exist in regions of the atmosphere which are sufficiently cold for them to activate to ice, we plot 3-monthly averaged seasonal distributions of INPs active at the ambient temperature ($[INP]_{ambient}$) along a transect through the Atlantic (at 30°W; Figure 4d). This plot suggests that marine organic sea spray may contribute significantly to cloud glaciation at high and mid latitudes during the wintertime in the respective hemispheres. It also shows the strong seasonal differences caused by temperature and source strength to the relative $[INP]_{ambient}$ contribution from marine and dust sources.

In summary, we show that surface active organic material from the microlayer which is similar to that found in sea spray aerosol, nucleates ice and we tentatively identify the ice active material as being connected to diatom exudates. Our findings also suggest that marine organic material may be an important global source of atmospheric INPs, particularly in areas remote from terrestrial sources such as the Southern Ocean. This work highlights the need for more field measurements of remote atmospheric INP concentration and its relationship to ocean surface water characteristics, including the local phytoplankton community, organic carbon concentrations and chemical characteristics, as well as the organic loading and nature of sea spray aerosol.

## References


1. Hoose, C. & Möhler, O. Heterogeneous ice nucleation on atmospheric aerosols: a review of results from laboratory experiments. *Atmos. Chem. Phys.* **12,** 9817–9854 (2012).

2. Murray, B. J., O'Sullivan, D., Atkinson, J. D. & Webb, M. E. Ice nucleation by particles immersed in supercooled cloud droplets. *Chem. Soc. Rev.* **41,** 6519–6554 (2012).

3. Bigg, E. K. Ice Nucleus Concentrations in Remote Areas. *J. Atmos. Sci.* **30,** 1153–1157 (1973).

4. Rosinski, J., Haagenson, P. L., Nagamoto, C. T. & Parungo, F. Nature of ice-forming nuclei in marine air masses. *J. Aerosol Sci.* **18,** 291–309 (1987).

5. Bigg, E. K. Ice forming nuclei in the high Arctic. *Tellus B* **48,** 223–233 (1996).

6. Knopf, D. A., Alpert, P. A., Wang, B. & Aller, J. Y. Stimulation of ice nucleation by marine diatoms. *Nat. Geosci.* **4,** 88–90 (2011).

7. Fall, R. & Schnell, R. C. Association of an ice-nucleating psuedomonad with cultures of the marine dinoflagellate, heterocapsa-niei. *J. Mar. Res.* **43,** 257–265 (1985).

8. Prather, K. A. *et al.* Bringing the ocean into the laboratory to probe the chemical complexity of sea spray aerosol. *Proc. Natl. Acad. Sci.* **110 ,** 7550–7555 (2013).

9. Yun, Y. & Penner, J. E. An evaluation of the potential radiative forcing and climatic impact of marine organic aerosols as heterogeneous ice nuclei. *Geophys. Res. Lett.* **40,** 4121–4126 (2013).

10. Burrows, S. M., Hoose, C., Pöschl, U. & Lawrence, M. G. Ice nuclei in marine air: biogenic particles or dust? *Atmos. Chem. Phys.* **13,** 245–267 (2013).

11. Wang, X. *et al.* Microbial Control of Sea Spray Aerosol Composition: A Tale of Two Blooms. *ACS Cent. Sci.* (2015). doi:10.1021/acscentsci.5b00148

12. Gantt, B. & Meskhidze, N. The physical and chemical characteristics of marine primary organic aerosol: a review. *Atmos. Chem. Phys* **13,** 3979–3996 (2013).

13. Aller, J. Y., Kuznetsova, M. R., Jahns, C. J. & Kemp, P. F. The sea surface microlayer as a source of viral and bacterial enrichment in marine aerosols. *J. Aerosol Sci.* **36,** 801–812 (2005).

14. Orellana, M. V *et al.* Marine microgels as a source of cloud condensation nuclei in the high Arctic. *Proc. Natl. Acad. Sci.* **108 ,** 13612–13617 (2011).

15. Schmitt-Kopplin, P. *et al.* Dissolved organic matter in sea spray: a transfer study from marine surface water to aerosols. *Biogeosciences* **9,** 1571–1582 (2012).

16. Russell, L. M., Hawkins, L. N., Frossard, A. A., Quinn, P. K. & Bates, T. S. Carbohydrate-like composition of submicron atmospheric particles and their production from ocean bubble bursting. *Proc. Natl. Acad. Sci. USA* **107,** 6652–6657 (2010).

17. Leck, C. & Bigg, E. K. Biogenic particles in the surface microlayer and overlaying atmosphere in the central Arctic Ocean during summer. *Tellus B* **57,** 305–316 (2005).

18. Cunliffe, M. *et al.* Sea surface microlayers: A unified physicochemical and biological perspective of the air–ocean interface. *Prog. Oceanogr.* **109,** 104–116 (2013).

19. Quinn, P. K. *et al.* Contribution of sea surface carbon pool to organic matter enrichment in sea spray aerosol. *Nat. Geosci* **7,** 228–232 (2014).

20. Cziczo, D. J. *et al.* Clarifying the Dominant Sources and Mechanisms of Cirrus Cloud Formation. *Science (80-. ).* **340,** 1320–1324 (2013).

21. Yakobi-Hancock, J. D., Ladino, L. A. & Abbatt, J. P. D. Feldspar Minerals as Efficient Deposition Ice Nuclei. *Atmos. Chem. Phys.* **13,** 11175–11185 (2013).

22. Kanji, Z. A., Welti, A., Chou, C., Stetzer, O. & Lohmann, U. Laboratory studies of immersion and deposition mode ice nucleation of ozone aged mineral dust particles. *Atmos. Chem. Phys.* **13,** 9097–9118 (2013).

23. Pummer, B. G., Bauer, H., Bernardi, J., Bleicher, S. & Grothe, H. Suspendable macromolecules are responsible for ice nucleation activity of birch and conifer pollen. *Atmos. Chem. Phys.* **12,** 2541–2550 (2012).

24. Augustin, S. *et al.* Immersion freezing of birch pollen washing water. *Atmos. Chem. Phys.* **13,** 10989–11003 (2013).

25. O′Sullivan, D. *et al.* The relevance of nanoscale biological fragments for ice nucleation in clouds. *Sci. Rep.* **5,** (2015).

26. Fröhlich-Nowoisky, J. *et al.* Ice nucleation activity in the widespread soil fungus Mortierella alpina. *Biogeosciences* **12,** 1057–1071 (2015).

27. Armbrust, E. V. The life of diatoms in the world's oceans. *Nature* **459,** 185–192 (2009).

28. Alvain, S., Moulin, C., Dandonneau, Y. & Loisel, H. Seasonal distribution and succession of dominant phytoplankton groups in the global ocean: A satellite view. *Global Biogeochem. Cycles* **22,** GB3001 (2008).

29. Fuentes, E., Coe, H., Green, D. & McFiggans, G. On the impacts of phytoplankton-derived organic matter on the properties of the primary marine aerosol – Part 2: Composition, hygroscopicity and cloud condensation activity. *Atmos. Chem. Phys.* **11,** 2585–2602 (2011).

30. Atkinson, J. D. *et al.* The importance of feldspar for ice nucleation by mineral dust in mixed-phase clouds. *Nature* **498,** 355–358 (2013).

31. Koop, T., Luo, B. P., Tsias, A. & Peter, T. Water activity as the determinant for homogeneous ice nucleation in aqueous solutions. *Nature* **406,** 611–614 (2000).

32. Alpert, P. A., Aller, J. Y. & Knopf, D. A. Ice nucleation from aqueous NaCl droplets with and without marine diatoms. *Atmos. Chem. Phys* **11,** 5539–5555 (2011).

## Acknowledgements

T.W.W., B.J.M. and T.F.W. acknowledge the assistance provided by the crew and other scientists on-board the RV Knorr and the RSS James Clark Ross, the British Antarctic Survey, K. Baustian, J. McQuaid, A. Windross, J. Knulst, J.F. Wilson, A.M. Booth, R. Chance, S. Peppe, D. O'Sullivan, N. Umo I. Cotton, H. Pearce, H. Price and M.J. Callaghan. The STXM/NEXAFS analysis was performed at the Advanced Light Source (ALS), Lawrence Berkeley National Laboratory supported by the Director, Office of Science, Office of Basic Energy Sciences, of the U.S. Department of Energy under Contract No. DE-AC02-05CH11231 (User award to Knopf/Aller ALS-05955). We thank A.L.D. Kilcoyne for assistance with STXM measurements. L.A.L. acknowledges assistance from R. Leaitch, E. Mungall, R. Christensen and J. Li and the Pacific region Department of Fisheries and Oceans staff. The Marine Boundary Layer sampling site in Ucluelet is jointly supported and maintained by Environment Canada, BC Ministry of the Environment and Metro Vancouver. We acknowledge funding from the Natural Environment Research Council (NE/K004417/1; NE/I020059/1; NE/I013466/1, NE/I028696/1, NE/I019057/1, NE/H009485/1), the European Research Council (FP7, 240449 ICE, BACCHUS 603445), the UK Aerosol Society, National Science Foundation (AGS-1232203), German Research Foundation (WU585/6-1), the Climate Change and Atmospheric Research Program of the Natural Sciences and Engineering Research Council of Canada (for NETCARE), Fisheries and Oceans Canada, Environment Canada, NOAA's Climate Program Office (for WACS II), and the DOE Office of Science (BER) Earth System Modeling Program.

## Author contributions

T.W.W. organised the ICE-ACCACIA campaign, designed experiments, collected and analysed samples during and after the campaign, managed collaborations and co-wrote this manuscript. L.A.L. designed experiments and analysed samples during the NETCARE campaign and co-wrote this manuscript. P.A.A. collected and analysed STXM/NEXAFS spectra and diatom exudate freezing data and contributed to manuscript writing. M.N.B. collected flow cytometry data for SML samples during ACCACIA. I.M.B. sought funding for ACCACIA and helped design the microlayer sampling procedure. S.M.B., J.V.T, J.B., and K.C. performed and analysed the model simulations. C.J. performed heating tests on ICE-ACCACIA samples. W.P.K. assisted with collection of material during WACSII cruise, provided exudate material for experiments, and participated in STXM/NEXAFS data collection. G.M., J.N. and S.R conducted TOC measurements on Arctic samples. L.A.M., O.W. and E.P. collected the Ucluelet, Line P and open ocean samples, and conducted the NETCARE biogeochemical analysis. C.L.S. helped organise the measurements at the Ucluelet site and facilitated the use of the sampling site. T.F.W. collected and analysed samples during and after the ICE-ACCACIA campaign and assisted with design of experiments. J.D.Y., J.A.H, R.M, M.S. and J.P.S.W. collected the Ucluelet samples and helped with the NETCARE experiments. A.K.B. and J.P.D.A. oversaw and organized the NETCARE field campaign and provided financial support for it. D.A.K. and J.Y.A. initiated and designed the STXM/NEXAFS and diatom exudate freezing experiments, contributed to the writing of this manuscript and provided financial support for WACSII cruise participation, exudate freezing experiments, and STXM/NEXAFS analyses. B.J.M. established the collaborations necessary for this paper, helped to write the paper and oversaw the ICE-ACCACIA campaign and sought funding for it.



The authors declare no competing financial interests.

Correspondence and requests for materials should be addressed to t.w.wilson@leeds.ac.uk and luis.ladinomoreno@utoronto.ca.

## Figure legends

Figure 1 **Sea spray aerosol particles enriched in organic material are generated when bubbles burst at the air-sea interface.** Surface active organic material of biological origin is scavenged at the interfaces of bubbles as they rise through the water column. This process enriches the air-sea interface with surface active organic material forming the sea surface microlayer (green layers). The organic material is ejected on bubble bursting with resulting sub-micron film drops being enriched with organic material compared to larger jet drops. We show that the biogenic organic material in the sea surface microlayer is likely an important source of atmospheric ice nucleating particles that could influence cloud properties.

Figure 2 **Ice nucleation by material in the sea surface microlayer (SML). a)** Immersion mode fraction frozen curves for 1 µl Arctic and Atlantic SML and sub-surface water (SSW) droplets determined using the µl-NIPI, with example temperature uncertainties included. **b)** The cumulative number of INPs per g of total organic carbon (TOC). Selected samples were diluted with ultra-pure water to 10 and 1% of initial concentration. Uncertainties included where error bars are larger than data points (see methods for details). Equation for fit to data is INPs per g TOC = exp[11.2186–0.4459*T(°C)]. **c)** Ice nucleation by BC coast and North Pacific samples under cirrus conditions. Example UT-CFDC activation curves under cirrus conditions (with background counts subtracted) for sea salt (SS), NaCl, BC coast SML and SSW samples at -40°C. **d)** Ice nucleation onset $RH_{ice}$ for Pacific and BC coast SML, SSW, SS and NaCl aerosol particles. For comparison onsets for Arizona test dust (ATD) and K-feldspar (orthoclase)[21] are shown. The solid line represents the water saturation line, and the dashed line is the theoretical homogeneous freezing threshold[31].

Figure 3 **Spectroscopic analysis of Arctic SML samples and freezing experiments with diatom exudate a)** and **b)** X-ray images of Arctic SML5 and 19, respectively. Example locations at which spectra were acquired are indicated by green and blue boxes. **c)** X-ray absorption spectra of organic material in SML5, SML9 and exudates from the diatom *Thalassiosira pseudonana*. **d)** Freezing and melting temperatures, collected using WACIFE, as a function of water activity ($a_w$) for nanolitre volume droplets containing *T. pseudonana* exudates, and filtered and autoclaved natural seawater with and without f/2 nutrients. Heterogeneous ice nucleation temperatures in the presence of diatom cells and homogeneous ice nucleation of aqueous NaCl droplets are shown for comparison[6,32]. Vertical error bars represent 10$^{th}$ and 90$^{th}$ percentiles of about 300 individual freezing events. Horizontal error bars indicate the uncertainty in $a_w$ of ±0.01.

Figure 4 **Global distribution of atmospheric marine biogenic INP. a)** Modelled distribution of INP concentration active at -15°C ($m^{-3}$) and surface level marine aerosol organic mass concentration (µg $m^{-3}$); the locations of Bigg[3] (circles) and Rosinski[4] (triangles) data are shown **b)** Comparison of model simulated INP concentration verses the Bigg[3] and Rosinski[4] measured concentration for the same location at the activation temperature of the measurements; open symbols are for K-feldspar only and solid symbols are for mineral dust + marine organic. Example error bars shown on red points based on spread in INPs per g TOC (see Figure 2b). **c**) Modelled distribution of marine biogenic INP concentrations active at -20°C at 850 hPa (corresponding to the altitude of high latitude mixed phase clouds). Black contours indicate the INPs from desert dust based on K-feldspar emissions[30]. **d**) Seasonal altitude profiles (expressed as pressure) showing $[INP]_{ambient}$ (INP concentration active at local temperature conditions) from marine sources (colour scale) and K-feldspar (black contours), for a transect from the South to North poles through the Atlantic (30°W).

## Methods

### Sea surface microlayer and subsurface water sampling

Sea surface microlayer sampling took place in the Arctic during the ACCACIA (Aerosol-Cloud Coupling and Climate Interactions in the Arctic) cruise (Extended data Figure 1a), in the Atlantic as part of the WACS II (Western Atlantic Climate Study II) cruise (Extended data Figure 1b) as well as in the Northeast Pacific and off the southern coast of BC, Canada as part of the NETCARE (NETwork on Climate and Aerosols: Addressing Key Uncertainties in Remote Canadian Environments) project (Extended data Figure 1c). See Extended data Table 1 for precise sampling locations.

During the ACCACIA campaign in the Arctic, microlayer sampling was conducted from the *RSS James Clark Ross* in both open waters and within leads in the marginal ice zone (Extended data Table 1 and Extended data Figure 1a). Microlayer samples were collected into borosilicate glass bottles from a hydrophilic Teflon film on a rotating drum fitted to the 'Interface II' remote-controlled sampling catamaran[33]. Subsurface water was sampled with Niskin bottles on a CTD (conductivity, temperature, depth) rig at the same locations, generally at a depth of ~2 m. To avoid potential contamination from the ship, the microlayer sampler was navigated to a distance of 75 to 200 m upwind of the stationary ship before sampling commenced. Due to rougher conditions during the WACS II campaign in the Atlantic, the Interface II was tethered to the CTD arm of the *RV Knorr* during microlayer sampling. Subsurface water was collected either using the direct uncontaminated ship input at 5m water depth or using a sampling container lowered over the side of the ship (for details see Extended data Table 1). During both campaigns, before and after microlayer sampling, seawater from the ship's uncontaminated supply was flushed through Interface II's sampling system to clear any previously collected microlayer. Samples of the 'flushing' water were collected and analysed and compared to the subsurface water using droplet freezing assays to check INPs from previous sampling had been removed (Extended data Figure 8). Microlayer samples for water activity and organic carbon analysis were frozen immediately after collection at -80°C.

During the NETCARE campaign, SML samples and corresponding SSW samples from water depths of 0.5 m to 1.0 m, were collected in the Northeast Pacific Ocean at three different locations (Extended data Table 1 and Extended data Figure 1c). The samples were collected using a glass plate[34] with the exception of BC coast SML3, which was collected using an autoclaved stainless steel screen[18]. All samples were stored in high-density polyethylene bottles. North Pacific samples (Pacific SML1, 2 and 3) were kept frozen at -20°C after collection, and prior to the experiment they were thawed and stored at 4°C in the dark. All other samples were stored at 4°C in the dark for no more than ten days before analysis.

### Effect of different sampling techniques on INP abundance in Pacific samples

BC coast samples SML3 and SML4 were sampled at the same location 1 hour apart but using metal mesh and glass plate techniques, respectively. There is a significant difference in the onset humidity of the two samples, with the onset of ice formation for BC coast SML3 occurring 13% $RH_{ice}$ lower than for BC coast SML4. With the time lag between collection of the two samples and because the methods sample different thicknesses of the SML (the metal plate collects layers 2-4 times thicker than those layers collected with glass plates[18]), it is not clear if the difference in their onset $RH_{ice}$ was due to the different sampling methods.

### Ice nucleation experiments during ACCACCIA, WACS II and NETCARE campaigns

Arctic and Atlantic surface microlayer and sub-surface water samples were analysed for the presence of INPs using the previously described[30,35] microlitre Nucleation by Immersed Particle Instrument (µl-NIPI). Briefly, droplets with a volume of $1.0 \pm 0.1$ µl were pipetted onto a hydrophobic microscope coverslip (Extended data Figure 9a) and cooled at a rate of 1 K $min^{-1}$ using a Grant-Asymptote EF600 cold stage (Extended data Figure 9b) until all droplets were frozen. The temperature at which individual droplets froze was recorded, with an uncertainty of ±0.4°C. Experiments were also performed using diluted microlayer samples (Arctic SML3, 6, 16 plus Arctic SML5 filtered at 0.2 µm and Arctic SML12 filtered at 10 µm) where 1 ml of microlayer was added to 9 ml (10% dilution) or 99 ml (1% dilution) of 18.2 MΩ cm distilled

water (Milli-Q®). The water activity ($a_w$) of Arctic microlayer and sub-surface water samples was measured at 25°C using an Aqualab Series 3 dew point activity meter.

Samples from the North Pacific and BC coast were analysed using the University of Toronto continuous flow diffusion chamber (UT-CFDC). Due to the high total submicron particle concentration of both the microlayer and sub-surface water samples ($10^6$ $cm^{-3}$ after drying, measured with a TSI 3782 condensation particle counter) they were diluted by a factor of ca. 20 with 18.2 MΩ $cm^{-1}$ water prior to atomization using a TSI 3076 atomizer. Water was removed by passing the sample flow through three diffusion dryers, and the particle concentration was further lowered by dilution (Extended data Figure 9c). 200 nm mobility diameter particles were selected using a differential mobility analyser (TSI 3081), with size-selected particle concentrations of ca. 100 $cm^{-3}$. The size-selected particles were exposed to ice supersaturated conditions at -40°C in the UT-CFDC to determine their ice nucleation onset humidities[36]. Particle counts from both channels (>0.5 µm and >5 µm) of the optical particle counter (Climet CI-20) were used to distinguish between interstitial aerosol particles and ice particles. The standard solutions consisted of 8 to 10 mg of NaCl (Sigma Aldrich, S2830) and commercial sea salt (Sigma Aldrich, S9883) dissolved in 50 ml of 18.2 MΩ cm water. Control experiments with filtered air were conducted in the field.

## Ice nucleation experiments with diatom exudates

For diatom exudate freezing experiments, axenic unialgal cultures of *T. pseudonana* were grown in flasks at 16-18 °C with a 14 h light:10 h dark cycle in 0.1 µm filtered and autoclaved seawater with f/2 nutrient addition[37]. Seawater was collected at a depth of about 0.5 m about 100 km off the coast of Long Island, NY[38]. After one week of growth, when concentrations reached ~$10^6$ cells $ml^{-1}$, cultures were filtered through a 0.1 µm pore size filter to remove the cells, yielding a suspension of diatom exudates.

Droplets of filtered diatom exudate were analysed using the WACIFE (water activity controlled immersion freezing experiment) instrument. Individual droplets were deposited in a grid pattern onto a hydrophobic glass plate. Additional droplets were generated from filtered and autoclaved natural seawater with and without f/2 nutrient addition[37] prior to diatom growth. Droplet $a_w$ was established by allowing the temperature-controlled droplets to come to equilibrium in a humidity controlled aerosol conditioning cell[6,39]. Droplets were then sealed from ambient air, setting the droplets' $a_w$ equal to the applied RH. Ice nucleation was observed at a cooling rate of 10 K $min^{-1}$ using a cryo-cooling stage coupled to an optical microscope (see schematic of process in Extended data Figure 9d). Droplet sizes ranged from 60-129 µm circle equivalent diameters (82 µm average). Individual droplet volumes were calculated from the spherical equivalent diameter derived from the digitally measured particle diameters corrected for the non-sphericity of the deposited particles and for different applied $a_w$. The total number of droplets at each investigated $a_w$ for seawater, seawater+f/2 droplets, and seawater+f/2+diatom exudates were 115, 143 and 131, respectively. Homogeneous ice nucleation was observed for droplets generated from the seawater with and without f/2. The median freezing temperatures shown in Figure 3d include $10^{th}$ and $90^{th}$ percentiles. Corresponding mean melting temperatures are shown with an uncertainty of 1 standard deviation. The uncertainty in $a_w$ is ±0.01. The ice melting curve (dashed line) and the volume corrected homogeneous freezing curve with an uncertainty in $a_w$ of ±0.01 shown as the solid black line and grey shaded area, respectively, is parameterized by Koop and Zobrist[40].

## Freezing depression correction for immersion mode experiments

Data from the Arctic, Atlantic and diatom exudate immersion mode experiments were adjusted to account for the freezing depression caused by dissolved salts in seawater. First, a freezing curve as a function of $a_w$ was constructed through the median freezing points following the $a_w$ criterion where median immersion freezing temperatures can be described by a horizontal shift in the ice melting curve[40]. Then the difference between expected median freezing temperatures for pure water (i.e. at $a_w$ =1.0) and at the experimentally applied $a_w$ were used as temperature offsets.

## Calculation of INPs per unit mass of organic carbon and associated uncertainty

In Figure 2b we show the show the cumulative number of INPs per g of TOC as a function of temperature for the Arctic and Atlantic microlayer samples. This calculation uses the time-independent singular description of ice nucleation[41] that assumes the time dependence of freezing is of secondary importance to the distribution of ice nucleating particle types. In this case 'INPs per g of TOC' is the same as '$n_m$' described in detail by Murray et al. (2012)[2]. It should also be noted that this is the same model that was used to calculate $n_s$[1] for the BC coast and North Pacific samples, but this describes the number of ice active sites per surface area rather than mass.

For all data points shown in Figure 2b error bars are based on the propagated uncertainties associated with volume measurements and organic carbon concentration measurements (Extended data Figure 7). The error bars for experiments in which microlayer samples were diluted with Milli-Q® water also include uncertainty relating to the subtraction of background heterogeneous nucleation events.

Freezing in µl-NIPI experiments using Milli-Q® water droplets free from any added nucleants occurs at higher temperatures than predicted for homogeneous ice nucleation[42]. Using the results of 22 separate freezing experiments (727 droplets in total) the cumulative number of INPs per volume of Milli-Q® was calculated. A line of best fit from this data as a function of temperature was used to estimate the number of background INPs present in our diluted microlayer samples. This value was subtracted from the diluted microlayer cumulative INP spectra and uncertainties relating to the variation in background INP concentrations were calculated based on the 68% confidence interval associated with the line of best fit.

## STXM/NEXAFS analysis of Arctic microlayer samples

Scanning Transmission X-ray Microscopy coupled with Near Edge Absorption Fine Structure Spectroscopy (STXM/NEXAFS) analysis was used to explore qualitatively the carbon functionality of organic material found in two Arctic SML samples (Arctic SML5 and 19). Analyses were performed at the Advanced Light Source on beamline 5.3.2.2 , Lawrence Berkeley National Laboratory[43]. An overview of the application of this technique to atmospheric particles and technical details on STXM methodology have been published elsewhere[44–50].The sample for STXM/NEXAFS analysis was collected by bringing the flat face of clean silicon nitride windows into contact with the pre-collected SML water surface and then lifting them off. Material adhering to the windows was allowed to air dry before examination. The transmission of soft single energy X-ray photons across the raster-scanned sample was measured to obtain an image[43] exploiting the carbon K-edge spectra to identify carbon functionality and the overall contribution of inorganic components. Using X-ray energies 278-320 eV, X-ray absorption of the ground state electron (1s orbital) of the carbon atom was probed to identify carbon-carbon double bonding (C=C), carbonyl (C=O), hydroxyl (C-OH) and carboxyl (COOH) functional groups. Figure 3a shows an X-ray image of particulate material found in the Arctic SML5 sample taken at 320 eV, which includes organic and inorganic material and a frustule fragment. The spectrum for SML5 is characterized by, i) a dominant carbonyl peak (288.2 eV), ii) a secondary carbon double bonding peak (285.4 eV), and iii) a gradual rise in absorption in the energy range where the hydroxyl functional group absorbs (287.3 eV). Abramson et al., (2009)[51] observed similar spectra for diatom cell wall material. The spectrum observed from SML19 is similar to that of the spectrum obtained from diatom exudates and characterized by i) a dominant carboxyl peak (288.6 eV) and ii) a gradual rise in absorption in the energy range where the hydroxyl functional group absorbs (287.3 eV). Similar spectral features have been observed by Hawkins and Russell (2010)[52] for field collected marine particles which they attribute to the presence of polysaccharides and by Ault et al., (2013)[53] for particles aerosolized from a laboratory breaking wave. These features were also observed in carbon absorption spectra by Zubavichus et al. (2005)[54] for 22 amino acids all of which are present in *T. pseudonana*[55], supporting the notion that diatom exudates were present in this microlayer sample. The presence of spectral features similar to diatom cell wall fragments and diatom exudates material suggests the presence of diatoms in both SML5 and SML19. It is important to note that marine SMLs[13,18,56–58], subsurface waters[59], and biofilms[60] are comprised of a complex mixture of inorganic particles, particulate organic matter in the form of microorganisms, biogenic debris, polysaccharide enriched microgels, lipids, proteins and amino acids. Therefore, the X-ray spectra

shown here will not be identical for different SML samples. Instead, key spectral features including peak locations and dominance, represent typical biogenically derived materials in the marine environment.

## Microlayer filtering and heating tests

A selection of fresh Arctic SML samples were passed through filters with a range of pore sizes (0.02 µm Whatman Anodisc, 0.1 µm Whatman Anodisc, 0.2 µm Sartorius Minisart, 0.45 µm Sartorius Minisart, 2.0 µm Millipore TTTP) and then tested for changes in immersion mode ice nucleating activity (Extended data Figure 2a). Selected NETCARE samples were filtered through 0.2 µm polyethersulfone membranes (IC Acrodisc) and then retested under cirrus conditions for ice nucleation activity (Extended data Figure 2b).

Selected Arctic and Atlantic samples were tested for immersion freezing activity after having been heated in a temperature controlled bath for 10 minutes. This was repeated at 8 temperatures between 20 and 100°C (Extended data Figure 2c). NETCARE samples, BC coast SML3 and Pacific SML1 were heated for 10 minutes at 100°C and retested under cirrus conditions for ice nucleation activity (Extended data Figure 2b).

## Flow cytometry (for ACCACIA SML samples)

Samples (2 mL) were transferred into a cryovial, and 50 µL of 50% glutaraldehyde was added to achieve a 0.5 % solution. The preserved sample was stored in the refrigerator for 30 minutes before snap-freezing in liquid nitrogen for storage at -80°C. Prior to analysis, samples were defrosted and the nucleic acid stain SYBR Green 1 dissolved in 300 mM potassium nitrate solution was added to achieve a 1% concentration of the stain (see Marie et al.[61] and Zubkov et al.[62] for more details). The samples were kept in the dark at room temperature for 1 hour. Bacterial abundance shown in Extended data Figure 4 was quantified using a flow cytometer (Becton Dickinson FACScan) following methods outlined in the literature[61,62].

## TOC, DOC and TEP characterisation

Transparent exopolymer particles (TEP, Extended data Figure 5b) concentrations were determined using spectrophotometric methods[63]. Samples (5-50 mL) of NETCARE SML and subsurface water were filtered immediately after sampling onto 0.2 µm polycarbonate membranes under low vacuum pressure (<100 mm Hg) and the membranes stained with 0.5 mL Alcian blue solution (0.02 g Alcian blue in 100 mL of acetic acid solution, pH 2.5), and rinsed twice with 1 mL of DI water. Membranes were subsequently extracted in 6 mL of 80% sulphuric acid ($H_2SO_4$) for 2 h to dissolve the dye, and the absorbance of extracts measured in a 1 cm cuvette at 787 nm with standardization using xanthan gum equivalents ($X_{eq}$) and conversion to µg C $L^{-1}$ using a factor of 0.63 based on the compilation of multiple studies using phytoplankton cultures[64].

For analysis of DOC[65] in the NETCARE samples from the North Pacific (Extended data Figure 5a), subsamples of 20 mL were filtered through 0.2 µm polycarbonate membranes and the filtrates preserved for later analysis with 4 µL $H_3PO_4$ per mL sample. Concentrations of DOC were quantified using a Shimadzu TOC-V analyser.

Organic carbon analysis was also performed on the Arctic microlayer samples (Extended data Figure 7). After filtering through 0.2 µm pore size Whatman Anodisc filters, DOC was measured using a Shimadzu TOC-V using previously described methods[66,67]. Due to high carbon concentration the Arctic microlayer samples for total organic carbon (TOC) analysis were diluted with 1 part sample to 2 parts deionised water. Total carbon analyser (TOC 5050A, Shimadzu) was used to measure total organic and inorganic carbon in each sample twice (with coefficient of variance between measurements <2%); the average of these measurements was taken.

Atlantic samples were also analysed for DOC; 40 ml of sample was filtered through a 25 mm GFF filter and stored in a glass septum bottle. The resulting supernatant was acidified to a pH of 1 with roughly 3 drops of pure HCl to react any inorganic carbon, and inhibit potential microbial degradation prior to analysis in the DOC analyser (Shimadzu TOC-L, ±1% precision). Prior to DOC collection each septum bottle and filtration apparatus was acid washed, and GFF filters pre-combusted for 5 hours at 450°C. POC was measured in

Atlantic samples by filtering SML through precombusted 25 mm GFF filters (0.7 micron pore size) prior to analysis (filters were frozen at -20°C until processing).

## Global modelling study

To assess the potential contribution of marine biogenic INP sources to the global atmospheric INP distribution we combined our experimental data from immersion mode experiments using the Arctic and Atlantic SML samples (the fit shown in Figure 2b) with a modelled distribution of emitted primary organic material in sea spray aerosol[10]. This was compared to desert dust INP concentrations based on emissions of K-feldspar[30].

Atmospheric marine POC (particulate organic carbon) distributions are taken from Burrows et al.[10]. Briefly, organic material (OM) in sea spray is related to emitted NaCl by an empirical, observationally-based enrichment factor, (OM_aer / NaCl_aer) / (OM_sea / NaCl_sea) = 500. Further, the OM fraction in emitted sea spray (OM_aer / (OM_aer + NaCl_aer)) was not allowed to exceed 76%; which was the maximum observed submicron organic sea spray fraction according to Vignati et al.[68]. Marine organic carbon is emitted in proportion to climatological POC as retrieved by the MODIS-Aqua satellite, transported as soluble $r$ =100 nm particles in the atmosphere, and removed by size-dependent wet and dry deposition processes. The OM distribution (using OM = OC*1.9) was shown by Burrows et al.[10] to be consistent with another global model study of atmospheric marine OM[68] and is within a factor of two of annual mean atmospheric measurements at Amsterdam Island (37°48'S, 77°34'E)[69] and Mace Head (53°20'N, 9°54'W)[68].

The distribution of dust INPs was based on Atkinson et al.[33] who used the the global aerosol processes model (GLOMAP). In this study we used GLOMAP-mode[70], a two-moment aerosol size-resolving scheme, which calculates particle mass and number in seven variable-size log-normal modes. The model is forced by ECMWF 6-hourly global meteorological analyses and was run at a resolution of 2.8 x 2.8, with 31 pressure levels extending to ~10 hPa. Dust emissions are taken from the AEROCOM daily resolved dust inventory for 2000[71]. Emissions are separated into a feldspar and bulk component using a mineralogical inventory[72]. Dust is emitted into the insoluble (or primary) size distribution and is aged to the soluble distribution via condensation of $SO_2$ and secondary organics after which it is subject to wet scavenging processes. Evaluation of modeled dust mass concentrations against surface observations (from the University of Miami network) show a model bias of ~30% with the majority of observations within a factor of 2 of the modeled mass[70].

Mineral dust INP concentrations (originating from K-feldspar) were calculated offline via the time independent model as discussed in Atkinson et al.[30]. K-Feldspar (assumed to be 35% of Feldspar volume) surface area and particle number was calculated assuming external mixing within the soluble modes.

Figure 4d shows seasonal modelled concentrations of marine (colour scale) and K-feldspar (contours) INPs that are active at the ambient model temperature. We refer to this concentration as $[INP]_{ambient}$ and it is a useful indicator of locations in which INP concentrations are sufficiently high and the temperatures sufficiently low to potentially influence clouds. Both marine and K-feldspar $[INP]_{ambient}$ were calculated using averaged daily temperatures and averaged monthly marine organic and K-feldspar emissions during the indicated periods (left panel: December/January/February, right panel: June/July/August). In both cases the parameterisations used are valid over a limited temperature range (see Figure 2b for marine INP, and Atkinson et al. (2013)[30] for K-feldspar). We did not extrapolate for INP concentrations at temperatures above the upper limits of the parameterisation, instead we assumed the aerosol had no ice nucleating activity at higher temperatures. Due to the INP numbers being cumulative as temperature decreases, the concentration of INPs at the lowest valid temperature of the parameterisations represent the lower limits for INP concentrations at temperatures colder than the valid range. Below -38°C we do not show $[INP]_{ambient}$ since in this regime homogeneous nucleation will dominate.

## Additional references


33. Knulst, J. C., Rosenberger, D., Thompson, B. & Paatero, J. Intensive sea surface microlayer investigations of open leads in the pack ice during Arctic Ocean 2001 expedition. *Langmuir* **19,** 10194–10199 (2003).

34. Wurl, O., Miller, L., Röttgers, R. & Vagle, S. The distribution and fate of surface-active substances in the sea-surface microlayer and water column. *Mar. Chem.* **115,** 1–9 (2009).

35. Whale, T. F. *et al.* A technique for quantifying heterogeneous ice nucleation in microlitre supercooled water droplets. *Atmos. Meas. Tech. Discuss.* **7,** 9509–9536 (2014).

36. Kanji, Z. A. & Abbatt, J. P. D. The University of Toronto Continuous Flow Diffusion Chamber (UT-CFDC): A Simple Design for Ice Nucleation Studies. *Aerosol Sci. Tech.* **43,** 730–738 (2009).

37. Guillard, R. R. L. & Ryther, J. H. Studies of marine planktonic diatoms: I. Cyclotella nana hustedt, and Detonula confervacea (cleve) gran. *Can. J. Microbiol.* **8,** 229–239 (1962).

38. Fisher, N. S. & Wente, M. The release of trace elements by dying marine phytoplankton. *Deep Sea Res. Part I Oceanogr. Res. Pap.* **40,** 671–694 (1993).

39. Alpert, P. A., Aller, J. Y. & Knopf, D. A. Initiation of the ice phase by marine biogenic surfaces in supersaturated gas and supercooled aqueous phases. *Phys. Chem. Chem. Phys.* **13,** 19882–19894 (2011).

40. Koop, T. & Zobrist, B. Parameterizations for ice nucleation in biological and atmospheric systems. *Phys. Chem. Chem. Phys.* **11,** 10839–10850 (2009).

41. Vali, G. Quantitative Evaluation of Experimental Results an the Heterogeneous Freezing Nucleation of Supercooled Liquids. *J. Atmos. Sci.* **28,** 402–409 (1971).

42. Murray, B. J. *et al.* Kinetics of the homogeneous freezing of water. *Phys. Chem. Chem. Phys.* **12,** 10380–10387 (2010).

43. Kilcoyne, A. L. D. *et al.* Interferometer-controlled scanning transmission X-ray microscopes at the Advanced Light Source. *J. Synchrotron Radiat.* **10,** 125–136 (2003).

44. Ghorai, S., Laskin, A. & Tivanski, A. V. Spectroscopic Evidence of Keto−Enol Tautomerism in Deliquesced Malonic Acid Particles. *J. Phys. Chem. A* **115,** 4373–4380 (2011).

45. Ghorai, S. & Tivanski, A. V. Hygroscopic Behavior of Individual Submicrometer Particles Studied by X-ray Spectromicroscopy. *Anal. Chem.* **82,** 9289–9298 (2010).

46. Moffet, R. C., Henn, T., Laskin, A. & Gilles, M. K. Automated Chemical Analysis of Internally Mixed Aerosol Particles Using X-ray Spectromicroscopy at the Carbon K-Edge. *Anal. Chem.* **82,** 7906–7914 (2010).

47. Moffet, R. C., Tivanski, A. V & Gilles, M. K. in *Fundam. Appl. Aerosol Spectrosc.* (Signorell, R. & Reid, J. P.) 419–462 (Taylor & Francis Group, LLC, 2010).

48. Hopkins, R. J., Tivanski, A. V, Marten, B. D. & Gilles, M. K. Chemical bonding and structure of black carbon reference materials and individual carbonaceous atmospheric aerosols. *J. Aerosol Sci.* **38,** 573–591 (2007).

49. Knopf, D. A. *et al.* Microspectroscopic imaging and characterization of individually identified ice nucleating particles from a case field study. *J. Geophys. Res. Atmos.* **119,** 2014JD021866 (2014).

50. Takahama, S., Gilardoni, S., Russell, L. M. & Kilcoyne, A. L. D. Classification of multiple types of organic carbon composition in atmospheric particles by scanning transmission X-ray microscopy analysis. *Atmos. Environ.* **41,** 9435–9451 (2007).

51. Abramson, L., Wirick, S., Lee, C., Jacobsen, C. & Brandes, J. A. The use of soft X-ray spectromicroscopy to investigate the distribution and composition of organic matter in a diatom frustule and a biomimetic analog. *Deep Sea Res. Part II Top. Stud. Oceanogr.* **56,** 1369–1380 (2009).

52. Hawkins, L. N. & Russell, L. M. Polysaccharides, Proteins, and Phytoplankton Fragments: Four Chemically Distinct Types of Marine Primary Organic Aerosol Classified by Single Particle Spectromicroscopy. *Adv. Meteorol.* (2010). doi:10.1155/2010/612132

53. Ault, A. P. *et al.* Size-Dependent Changes in Sea Spray Aerosol Composition and Properties with Different Seawater Conditions. *Environ. Sci. Technol.* **47,** 5603–5612 (2013).

54. Zubavichus, Y., Shaporenko, A., Grunze, M. & Zharnikov, M. Innershell Absorption Spectroscopy of Amino Acids at All Relevant Absorption Edges. *J. Phys. Chem. A* **109,** 6998–7000 (2005).

55. Brown, M. R. The amino-acid and sugar composition of 16 species of microalgae used in mariculture. *J. Exp. Mar. Bio. Ecol.* **145,** 79–99 (1991).

56. Kuznetsova, M., Lee, C. & Aller, J. Characterization of the proteinaceous matter in marine aerosols. *Mar. Chem.* **96,** 359–377 (2005).

57. Van Pinxteren, M., Müller, C., Iinuma, Y., Stolle, C. & Herrmann, H. Chemical Characterization of Dissolved Organic Compounds from Coastal Sea Surface Microlayers (Baltic Sea, Germany). *Environ. Sci. Technol.* **46,** 10455–10462 (2012).

58. Verdugo, P. Marine Microgels. *Ann. Rev. Mar. Sci.* **4,** 375–400 (2011).

59. Brandes, J. A. *et al.* Examining marine particulate organic matter at sub-micron scales using scanning transmission X-ray microscopy and carbon X-ray absorption near edge structure spectroscopy. *Mar. Chem.* **92,** 107–121 (2004).

60. Lawrence, J. R. *et al.* Scanning Transmission X-Ray, Laser Scanning, and Transmission Electron Microscopy Mapping of the Exopolymeric Matrix of Microbial Biofilms. *Appl. Environ. Microbiol.* **69 ,** 5543–5554 (2003).

61. Marie, D., Partensky, F., Jacquet, S. & Vaulot, D. Enumeration and Cell Cycle Analysis of Natural Populations of Marine Picoplankton by Flow Cytometry Using the Nucleic Acid Stain SYBR Green I. *Appl. Environ. Microbiol.* **63,** 186–193 (1997).

62. Zubkov, M. V, Burkill, P. H. & Topping, J. N. Flow cytometric enumeration of DNA-stained oceanic planktonic protists. *J. Plankton Res.* **29,** 79–86 (2007).

63. Engel, A. in *Pract. Guidel. Anal. Seawater* (O. Wurl) 125–142 (CRC Press, 2009). doi:doi:10.1201/9781420073072.ch7

64. Engel, A. in *Deep Sea Res. Part I Oceanogr. Res. Pap.* **51,** 83–92 (2004).

65. Wurl, O. & Sin, T. in *Pract. Guidel. Anal. Seawater* (Wurl, O.) 33–48 (CRC Press, 2009).

66. Pan, X. *et al.* Dissolved organic carbon and apparent oxygen utilization in the Atlantic Ocean. *Deep Sea Res. Part I Oceanogr. Res. Pap.* **85,** 80–87 (2014).

67. MacGilchrist, G. A. *et al.* Effect of enhanced pCO2 levels on the production of dissolved organic carbon and transparent exopolymer particles in short-term bioassay experiments. *Biogeosciences* **11,** 3695–3706 (2014).

68. Vignati, E. *et al.* Global scale emission and distribution of sea-spray aerosol: Sea-salt and organic enrichment. *Atmos. Environ.* **44,** 670–677 (2010).

69. Sciare, J. *et al.* Long-term observations of carbonaceous aerosols in the Austral Ocean atmosphere: Evidence of a biogenic marine organic source. *J. Geophys. Res. Atmos.* **114,** (2009).

70. Mann, G. W. *et al.* Description and evaluation of GLOMAP-mode: a modal global aerosol microphysics model for the UKCA composition-climate model. *Geosci. Model Dev.* **3,** 519–551 (2010).

71. Huneeus, N. *et al.* Global dust model intercomparison in AeroCom phase I. *Atmos. Chem. Phys.* **11,** 7781–7816 (2011).

72. Nickovic, S., Vukovic, A., Vujadinovic, M., Djurdjevic, V. & Pejanovic, G. Technical Note: High-resolution mineralogical database of dust-productive soils for atmospheric dust modeling. *Atmos. Chem. Phys.* **12,** 845–855 (2012).

## Extended data legends

Extended data Table 1. **Details of the sampled sea surface microlayers and subsurface sea waters.** Details are given of samples collected during the ACCACIA Arctic cruise, WACS II Atlantic cruise and the NETCARE project. NE Pacific samples were collected as part of the Line P time series, cruise 2013-17. BC coast samples were collected in Terrace Bay on the western coast of Vancouver Island (BC, Canada) and at a location ca. 3 km offshore from Ucluelet. Location numbers relate to the maps shown in Extended data Figure 1.

Extended data Figure 1. **Sampling locations** Sea surface microlayer (SML) and subsurface water samples were collected during the ACCACIA campaign at Arctic sampling stations at the locations marked with solid red circles. Also shown are sampling locations during the WACS II campaign in the North Atlantic Ocean. NETCARE samples were collected at locations in the NE Pacific (yellow star and the green square, CCGS JP Tully, 14-19 June, 2013). The red diamond and blue asterisk correspond to the sampling locations for the NETCARE BC coastal samples (12-15 August, 2013). The inset is a zoom of the BC coast sampling locations.

Extended data Figure 2. **Effects of heating and filtering on the ice nucleation activity of microlayer samples. a)** The effect of filtering through different pore-sized filters on the temperature at which 50% of droplets had frozen ($T_{50}$) of Arctic and Atlantic SML samples tested using the µl-NIPI. Shaded grey area is the range of $T_{50}$ found for fresh unfiltered SSW during the campaign. **b)** Comparison of the UT-CFDC onset $RH_{ice}$ of unfiltered, filtered (0.2 µm) and heated (to 100°C for 10 minutes) North Pacific and BC coast SML and SSW samples. The blue lines, and the red and dark blue symbols are as shown in Figure 2d. The green symbols represent the filtered onsets, whereas the black symbols represent the heated results. **c)** Results of heating tests using Arctic and Atlantic SML samples on $T_{50}$ tested using the µl-NIPI. Shaded grey area is the range of $T_{50}$ found for fresh untreated Arctic SSW.

Extended data Figure 3. **Ice surface site densities for the Pacific microlayer samples.** Comparison of the ice surface densities ($n_s$) calculated from UT-CFDC data for the NETCARE SML samples with literature data. The $n_s$ values were obtained at -40°C assuming that the particles were spherical. The SML $n_s$ values are indicated by the colored symbols, whereas the mineral dust $n_s$ values are indicated by the grey symbols. The dark grey and light grey symbols are from Yakobi-Hancock et al.[21] and Kanji et al.[22], respectively.

Extended data Figure 4 **Bacterial cell counts for Arctic samples. a)** Bacterial cell counts from flow cytometry performed on Arctic SSW (black squares), fresh Arctic SML (red circles). **b)** The SML sample cell counts plotted against $T_{50}$ (temperature at which 50% of droplets frozen) and line of best fit, $R^2 = 0.29$.

Extended data Figure 5. **Correlation of TEP and DOC with the UT-CFDC $RH_{ice}$ onsets.** Ice nucleation $RH_{ice}$ onsets for NE Pacific (see Extended data Table 1) samples plotted against **a)** measured DOC concentration, and **b)** TEP enrichment factor.

Extended data Figure 6. **Ice nucleating activity of diatoms cells and their exudates.** WACIFE (water activity controlled immersion freezing experiment) frozen fraction curves derived from 60-129 μm sized droplets (~0.4 nl volume) as a function of temperature. Green symbols indicate diatom exudates in 0.1 μm filtered seawater. Blue and red symbols represent 0.1 μm filtered seawater devoid of exudates with and without the addition of growth media, respectively. All temperatures have been corrected for freezing point depression to pure water conditions from their initial aqueous solution water activity, $a_w$ = 0.985 (open circles), 0.97 (open squares), 0.96 (filled diamonds), 0.95 (open diamonds), 0.94 (filled circles), 0.925 (open triangle), 0.90 (asterisks). Shaded areas illustrate ranges of observed heterogeneous ice nucleation of intact and fragmented diatom cells (green) and homogeneous ice nucleation of aqueous NaCl droplets (grey) for similar $a_w$ values[6,32]. Predicted homogeneous freezing temperatures for similar sized water droplets are indicated by the grey bar[31,40].

Extended data Figure 7 **TOC and DOC measurements for Arctic samples.** Arctic microlayer TOC and DOC measurements and Arctic subsurface water DOC measurements. For comparison here we provide the Atlantic TOC measurements; Atlantic SML1 = 5.954±0.185 mg $l^{-1}$, Atlantic SML2 = 4.643±0.135 mg $l^{-1}$.

Extended data Figure 8. **μl-NIPI Freezing curves for Arctic and Atlantic samples uncorrected for freezing depression caused by salts** Fraction frozen curves for 1 μl droplet freezing experiments using Arctic and Atlantic ocean samples, uncorrected for freezing point depression. SML, SSW and boat flushing water (grey points, symbols correspond to those for SML sampled at the same locations) to check for the absence of contaminant ice nuclei prior to sampling).

Extended data Figure 9. **Summary of ice nucleation experimental setups a)** Pipetting 1 μl droplets onto a hydrophobic glass slide. **b)** Schematic of the μl-NIPI cold stage used for immersion mode droplet freezing experiments. **c)** Schematic of the experimental setup for cirrus cloud relevant experiments. DMA: differential mobility analyzer; UT-CFDC: University of Toronto continuous flow diffusion chamber; CPC: condensation particle counter; OPC: optical particle counter, and **d)** Schematic of the water activity controlled immersion freezing experiment (WACIFE) for freezing of micrometer sized droplets containing diatom exudates as a function of water activity, $a_w$, and relative humidity, RH. Images are not to scale. The procedure for preparing and freezing droplets of filtered and autoclaved natural seawater with and without added f/2 nutrients droplets is similar except 0.1 μm filtration is not required

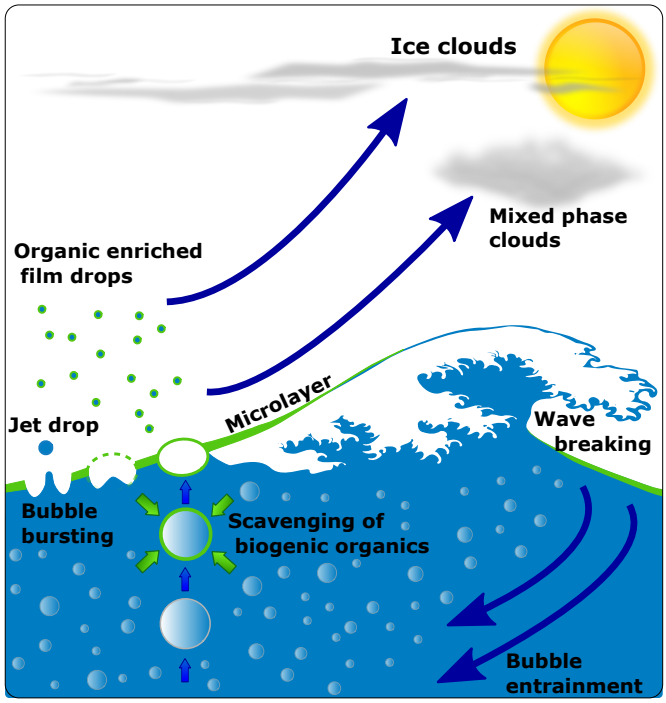
Ice clouds
Mixed phase clouds
Organic enriched film drops
Microlayer
Jet drop
Wave breaking
Bubble bursting
Scavenging of biogenic organics
Bubble entrainment

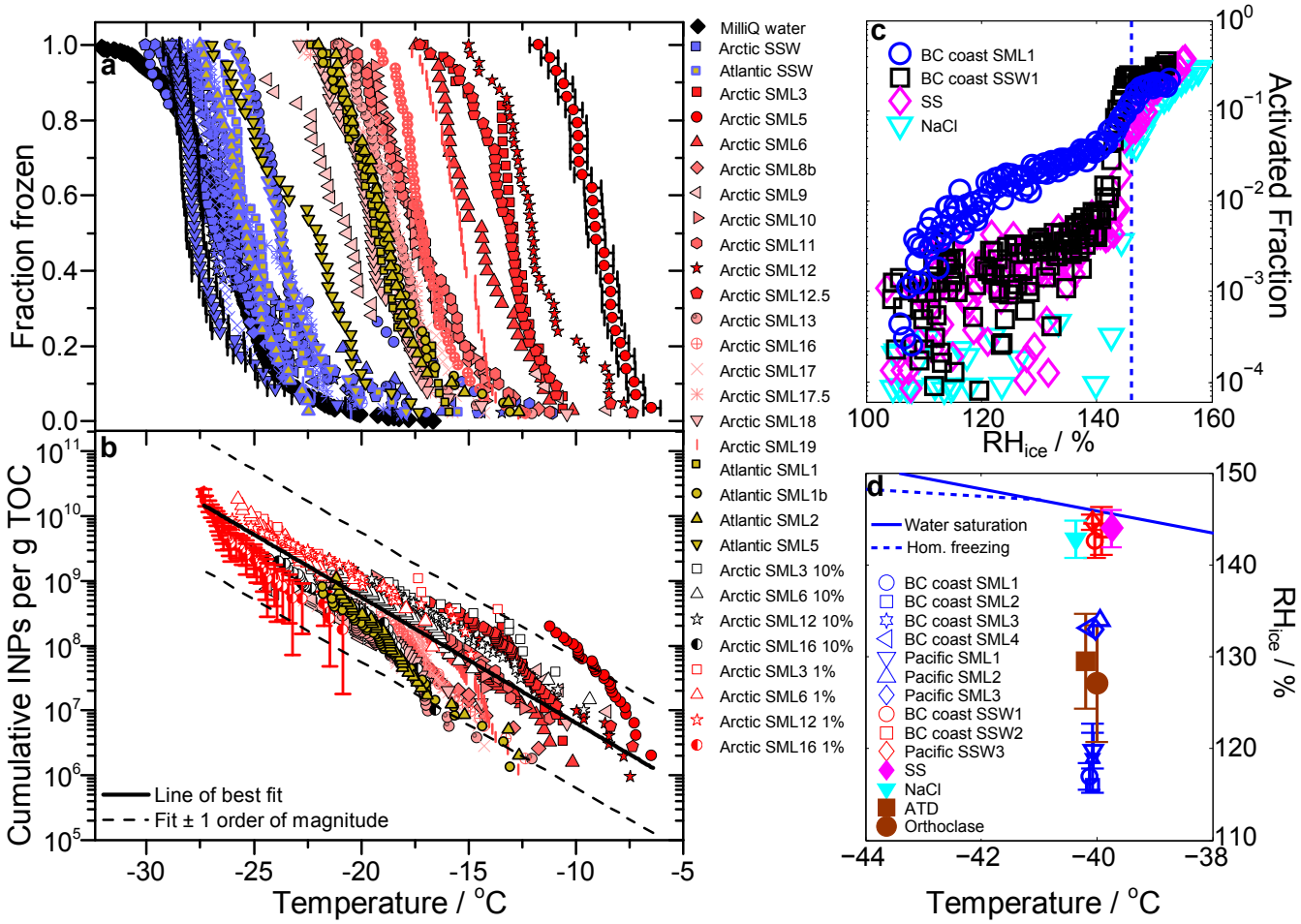
a
b
c
d
Fraction frozen
Cumulative INPs per g TOC
Temperature / °C
Line of best fit
Fit ± 1 order of magnitude
MilliQ water
Arctic SSW
Atlantic SSW
Arctic SML3
Arctic SML5
Arctic SML6
Arctic SML8b
Arctic SML9
Arctic SML10
Arctic SML11
Arctic SML12
Arctic SML12.5
Arctic SML13
Arctic SML16
Arctic SML17
Arctic SML17.5
Arctic SML18
Arctic SML19
Atlantic SML1
Atlantic SML1b
Atlantic SML2
Atlantic SML5
Arctic SML3 10%
Arctic SML6 10%
Arctic SML12 10%
Arctic SML16 10%
Arctic SML3 1%
Arctic SML6 1%
Arctic SML12 1%
Arctic SML16 1%
BC coast SML1
BC coast SSW1
SS
NaCl
Activated Fraction
RHice / %
Water saturation
Hom. freezing
BC coast SML1
BC coast SML2
BC coast SML3
BC coast SML4
Pacific SML1
Pacific SML2
Pacific SML3
BC coast SSW1
BC coast SSW2
Pacific SSW3
SS
NaCl
ATD
Orthoclase
RHice / %
Temperature / °C

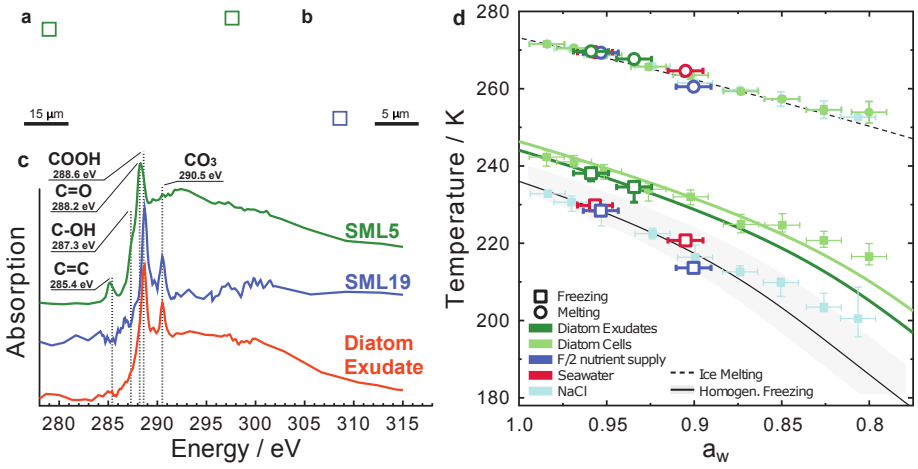
a
b
15 µm
5 µm
c
COOH
288.6 eV
C=O
288.2 eV
C-OH
287.3 eV
C=C
285.4 eV
CO3
290.5 eV
SML5
SML19
Diatom
Exudate
Absorption
280 285 290 295 300 305 310 315
Energy / eV
d
Temperature / K
280 260 240 220 200 180
1.0 0.95 0.9 0.85 0.8
aw
Freezing
Melting
Diatom Exudates
Diatom Cells
F/2 nutrient supply
Seawater
NaCl
Ice Melting
Homogen. Freezing

a) Surface level marine $[INP]_{-15}$ and (OC conc.)

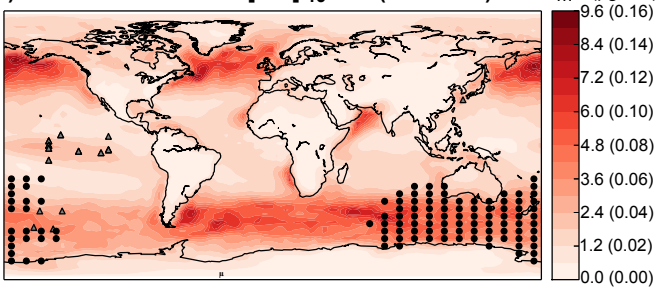


b) Simulated vs. observed INP concentrations

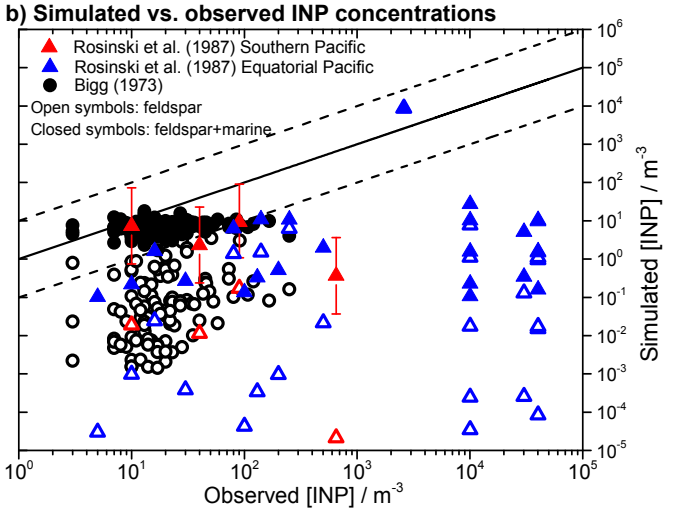


c) 850 hPa marine and feldspar $[INP]_{-20}$

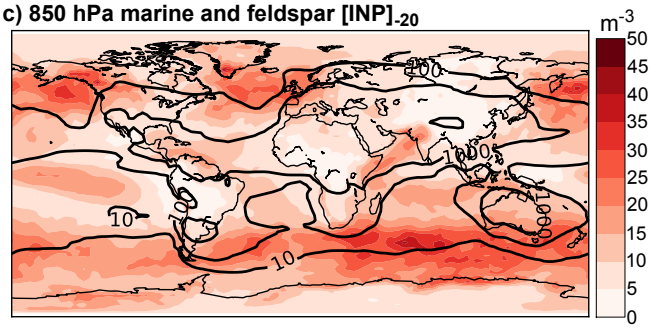


d) Marine and feldspar $[INP]_{ambient}$ seasonal Atlantic transect